EPJ Web of Conferences **35**, 01001 (2012)
DOI: 10.1051/epjconf/20123501001

A study of soil formation rates using ^{10}Be in the wet-dry tropics of northern Australia

R. Lal[1], L. K. Fifield[1], S.G. Tims[1], R.J. Wasson[2] and D. Howe[3]

[1]Department of Nuclear Physics, The Australian National University, ACT 0200, Australia
[2]Department of Geography, National University of Singapore AS2, #04-321 Arts Link, Singapore 117570
[3]Charles Darwin University, Darwin, NT, 0810, Australia

Abstract. A catchment level study to obtain soil formation rates using beryllium-10 (^{10}Be) tracers has been undertaken in the Daly River Basin in the wet-dry tropics of northern Australia. Three soil cores have been collected to bedrock, with depths ranging from ~1-3.5 m. Due to agricultural practices, modern soil loss rates can be significantly higher than long-term soil formation rates, but establishing soil formation rates has proved to be a difficult problem. At long-term equilibrium, however, soil formation from the underlying rock is balanced by soil loss from the surface. This long-term rate at which soil is being lost can be determined using the cosmogenic tracer ^{10}Be, created in spallation of atmospheric nitrogen and oxygen by cosmic rays. Since the annual fallout rate of ^{10}Be is known, the complete ^{10}Be inventory over the depth of the top soil can be used to establish the soil formation rates.

1 Introduction

Soil erosion of agricultural lands in Australia exceeds soil formation by factors up to three orders of magnitude [1]. The database of soil formation rates is, however, slim [2-4]. In order to expand this limited data base, in this study we look at a site, with a monsoonal climate, in the Daly Basin in Northern Territory, Australia.

Establishing 'natural' soil formation rates in relatively undisturbed sites allows a baseline to be determined against which denudation rates in agricultural landscapes can be assessed [5]. We use meteoric beryllium-10 (^{10}Be) to determine Quaternary soil production rates. We compare these rates with previously reported modern rates of soil loss on farms determined from ^{239}Pu measurements to assess if current soil loss rates are sustainable in this environment.

Meteoric ^{10}Be is a radioactive cosmogenic isotope primarily produced by the spallation of oxygen and nitrogen in the upper atmosphere [6]. After production the particle reactive BeO or $Be(OH)_2$ adheres to aerosols and falls out in precipitation or as dry deposition [7]. It adsorbs on to soil particles and accumulates in the upper meters of the soil profile where it decays with a half life of 1.39 Ma [8, 9]. The accumulated concentration of the nuclide in a surficial deposit serves as a proxy for the age and stability of the surface and it has been used as a tool to measure first-order soil erosion rates and residence times [10, 11].

Recent progress in characterizing the atmospheric production and fallout of ^{10}Be by numeric models agrees with present day measurements in rainfall and paleo-archives such as ice cores [12]. Short term variations in ^{10}Be delivery and solar modulation of cosmic rays have been shown to average out over the time scales at which soils accumulate [12]. Soil production rates obtained from this technique are therefore robust and insensitive to such short term modulations.

2 Background

^{10}Be binds firmly to soil particles after deposition. If this beryllium is retained in the soil, i.e. not carried away in solution then the only loss mechanisms are erosion and radioactive decay. At steady state with zero erosion the inventory of ^{10}Be is determined by balance between fallout and decay, and is given by

$$N_o = Q / \lambda \quad (1)$$

Where N_o is the inventory of ^{10}Be in atoms/cm^2, Q is the fallout rate in atoms/cm^2/year, and λ is the decay constant of ^{10}Be (4.99×10^{-7}/year). When soil is being lost by erosion the steady state inventory equation becomes

$$N_o = (Q - \epsilon\eta) / \lambda \quad (2)$$

Where ϵ is the erosion rate in g/cm^2/year and η is the ^{10}Be concentration in the eroded material in atoms/g.

Note: This method is independent of the shape of the ^{10}Be profile, as it uses the total inventory through the entire soil column.

3 Method

3.1 Sample Sites

The study site located at ~13° 50' S, 131° 13' E, is 250 km south of Darwin, in the Daly River Basin (52 577 km^2), near the confluence of the Daly and Douglas Rivers (figure 1). The catchment landscape is characterized by gently undulating limestone plains with low relief (< 100 m) and scattered lateritic low plateau Cretaceous remnants (mesas) and rocky hills [13]. Natural vegetation cover mainly consists of Eucalypt (*E. Miniata and E. Tetradonta*) woodlands and is retained on about 90 % of the Douglas-Daly area [14]. The basin has a monsoonal wet-dry climate and receives 1200 mm of rainfall annually, 90% of which occurs between November and March [15]. The region has been identified as suitable for large scale dry-land agriculture [16, 17].

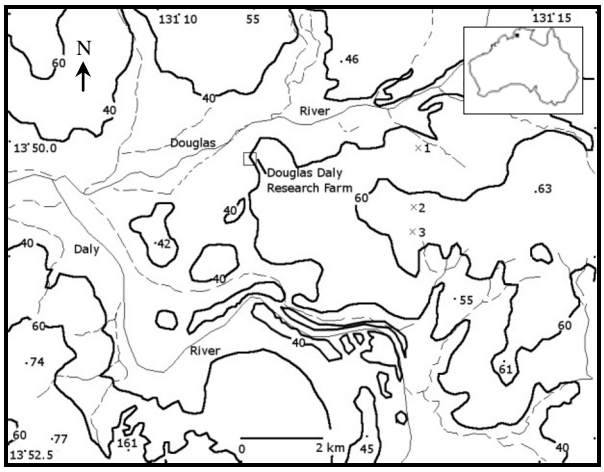

Fig. 1. Topographic map showing the location of the study sites (x). Note the contours are in (m) and drainage lines are indicated by --.

The bedrock formation underlying most of the Daly Basin is the ~190 m thick Oolloo Dolostone (A carbonate rock of ooid and stromatolitic dolostone and minor dolomitic sandstone) of Cambrian-Ordovician age [18]. A distinctive unconsolidated red loamy soil (Australian Soil Classification: Haplic Mesotrophic Red Kandosol) has developed *in-situ* over the Oolloo Dolostone [16, 18, 19]. This soil is generally deep and well-drained with a dark reddish brown, sandy loam A horizon up to 40 cm thick, and a massive dark red sandy clay loam and light clay B horizon extending > 2 m [19]. A sharp transition boundary exists between solum and bedrock and the poorly developed saprolite layer is indistinguishable from the solum.

The core samples were taken down a hillslope transect of ~ 2^o slope (figure 1). A rotary corer was used to drill a 10 cm diameter soil core down to bed rock at the three sites. The cores were relatively homogenous dark red loamy red earths, with weakly defined A (~ 0-25 cm) and B (> 25 cm) horizons. The solum was sampled in ~ 25 cm increments down to the bedrock.

3.2 Sample preparation and AMS measurements of ^{10}Be

After oven drying samples were reduced to ~ 100 g using a soil splitter. This sample was homogenized by grinding and a ~0.5 g subsample was taken for further processing using the fusion method [20]. The dry samples were weighed into 30ml Pt crucibles and ~ 0.5 mg of ^9Be tracer added as $^9BeCl_2$ solution before drying at 50°C for 2 h. A flux of anhydrous KHF_2 and anhydrous Na_2SO_4 were added to the crucibles at ratios of 5:1 and 1:1 relative to the sample weight, respectively. The crucible contents were mixed thoroughly and fused over a MAPP gas flame at ~2000 °C, producing a clear fluid melt within 1-2 min. The fusion converts the Be to the highly soluble BeF_4^{2-} anion which was extracted with water. K was removed as $KClO_4$ by precipitating with perchloric acid and B was reduced and the fluoroberyllate complex broken up by drying down with perchloric acid. The dry residue was dissolved in 1% HNO_3 and the Be was precipitated as $Be(OH)_2$ using a 1:3 ammonia solution. The precipitate was baked at 850 °C to convert it to BeO.

$^{10}Be/^9Be$ ratios were measured by accelerator mass spectrometry at the 14UD Heavy Ion Accelerator facility at the ANU [21]. $^{10}Be^{16}O^-$ and $^9Be^{16}O^-$ ions were selected sequentially by the mass-analyzing magnet after the ion source and injected into the accelerator operating at 8 MV. At the high voltage terminal the molecules were dissociated by low pressure oxygen gas, which also stripped electrons from the fragments converting the negative to positive ions. These positive ions were further accelerated to ground potential and $^{10}Be^{3+}$ or $^9Be^{3+}$ at an energy of 27 MeV was selected using a second magnet. The ^9Be beam current was measured on a Faraday cup after the magnet, while the ^{10}Be ions were counted individually with a gas filled ionization detector. The ^{10}Be ions were separated from ions of the ^{10}B isobar by exploiting the difference in range of the two ions. An argon gas cell inserted in front of the gas filled ionization detector was used to absorb the ^{10}B ions while allowing the ^{10}Be ions to pass through into the detector [22]. The $^{10}Be/^9Be$ ratios were standardized using the NIST SRM 4325 standard with an assumed $^{10}Be/^9Be$ ratio of 3.00×10^{-11}. The ^{10}Be content in the sample was determined from the measured $^{10}Be/^9Be$ ratios, the sample mass and the mass of ^9Be tracer used.

4 Results

The depth profiles of meteoric ^{10}Be in the cores are presented in figures 2-4 and in Tables 1-3. ^{10}Be is found to permeate the soil profile down to bedrock and a distinct mid depth maximum in the ^{10}Be concentration is observed. Soils with an eluviated clay rich subsurface B_t horizon, as in these kandosols, have been previously observed to have a mid-depth maximum ^{10}Be concentration [23]. The mid-depth maximum is probably due to smaller clay grain sizes which typically have a greater surface area per unit mass and enhanced ion exchange capabilities [24].

4.1 Site 1

The ^{10}Be concentration is nearly constant with depth with a surface concentration of 10.9×10^8 atoms/g, and a slight mid-depth maximum at 163.5 cm, of 13.3×10^8 atoms/g, below which it gradually declines except for a small increase at 335 cm where the bed rock interface is reached.

The ^{10}Be inventory was calculated using the average measured soil density of 1.6 ± 0.1 g/cm^3. The fallout at the study site is estimated to be 0.5 ± 0.1 (× 10^6) atoms /cm^2/year, based on the average global ^{10}Be flux map presented in [12]. This estimate incorporates dry and wet deposition with atmospheric circulation models and agrees with present day measurements and paleo-archives (*see* Table 1 of reference [12]). The ^{10}Be inventory in the soil column is 4.84 × 10^{11} atoms /cm^2, which is 48% of the cosmogenic steady sate inventory (CSI), calculated using Eq. 1. The measured inventory represents a minimum soil accumulation time of at least 968 ka.

Table 1. ^{10}Be results for Site 1.

Depth (cm) Site 1	^{10}Be (atoms/g) $\times10^8$	^{10}Be (atoms/cm^2) $\times10^8$	^{10}Be (atoms/cm^2) $\times10^8$ cumulative
0-25	10.9 ± 0.3	436 ± 14	436
25-50	13.1 ± 0.4	523 ± 16	960
50-75	12.3 ± 0.4	490 ± 15	1450
75-101	12.6 ± 0.4	525 ± 16	1975
101-126	12.4 ± 0.4	495 ± 16	2470
126-151	12.8 ± 0.4	510 ± 16	2980
151-176	13.3 ± 0.4	531 ± 16	3512
176-197	11.1 ± 0.3	373 ± 12	3884
197-222	6.7 ± 0.2	270 ± 9	4154
222-247	3.9 ± 0.1	156 ± 5	4310
247-272	4.0 ± 0.1	160 ± 5	4469
272-297	2.8 ± 0.1	111 ± 4	4581
297-310	3.0 ± 0.1	63 ± 2	4644
310-335	4.7 ± 0.7	187 ± 26	4830
335-360	0.20 ± 0.03	7 ± 1	4838
360-367	0.10 ± 0.01	0.6 ± 0.1	4838 ± 52

Table 2. ^{10}Be results for Site 2.

Depth (cm) Site 2	^{10}Be (atoms/g) $\times10^8$	^{10}Be (atoms/cm^2) $\times10^8$	^{10}Be (atoms/cm^2) $\times10^8$ cumulative
0-25	4.7 ± 0.2	187 ± 7	187
25-50	11.0 ± 0.4	438 ± 15	625
50-75	12.1 ± 0.4	486 ± 15	1111
75-97	13.7 ± 0.4	481 ± 15	1592
97-122	9.5 ± 0.3	382 ± 12	1974
122-147	15.2 ± 0.5	608 ± 19	2581
147-172	14.7 ± 0.5	588 ± 18	3169
172-195	13.9 ± 0.4	513 ± 16	3682
195-220	13.0 ± 0.4	518 ± 16	4200
220-245	11.8 ± 0.4	472 ± 15	4672
245-270	9.0 ± 0.3	360 ± 11	5032
270-282	8.6 ± 0.3	165 ± 5	5198
282-307	6.4 ± 0.2	257 ± 9	5455
307-332	8.0 ± 0.3	320 ± 10	5774
332-354	10.4 ± 0.3	367 ± 12	6142
354-370	0.50 ± 0.03	12 ± 1	6153 ± 53

Table 3. ^{10}Be results for Site 3.

Depth (cm) Site 3	^{10}Be (atoms/g) $\times10^8$	^{10}Be (atoms/cm^2) $\times10^8$	^{10}Be (atoms/cm^2) $\times10^8$ cumulative
0-25	5.5 ± 0.2	221 ± 7	221
25-50	7.6 ± 0.3	306 ± 10	527
50-65	10.1 ± 0.3	241 ± 8	768
65-90	8.4 ± 0.3	334 ± 11	1103 ± 19

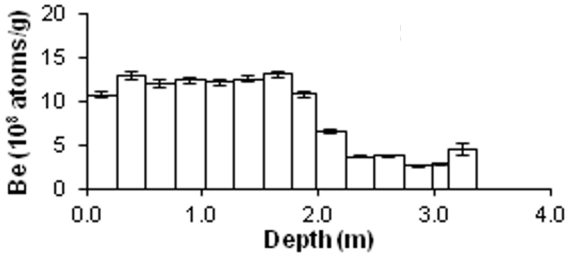

Fig. 2. Depth profile of ^{10}Be concentrations at Site 1.

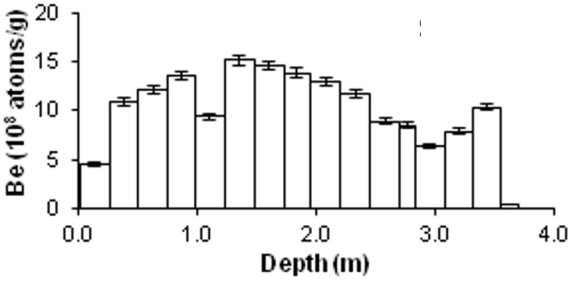

Fig. 3. Depth profile of ^{10}Be concentrations at Site 2.

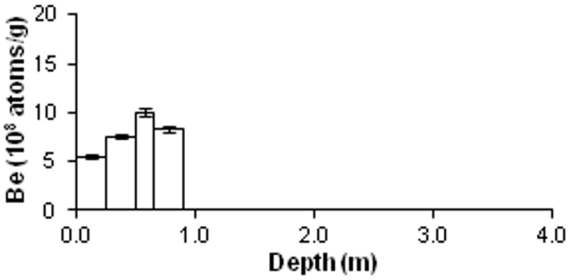

Fig. 4. Depth profile of ^{10}Be concentrations at Site 3.

4.2 Site 2

Unlike the relatively flat profile at Site 1, the ^{10}Be concentration at Site 2 reaches a pronounced maximum of 15.2 $\times 10^8$ atoms/g at a depth 134.5 cm, nearly 3 times the surface concentration of 4.7×10^8 atoms/g. The concentration then declines gradually but again rebounds slightly near the bedrock interface at 354 cm. The increase in ^{10}Be concentration at the solum-bedrock interfaces may be due to the lateral movement of ground water on the bedrock concentrating ^{10}Be rich particle fractions. The measured inventory of ^{10}Be of 6.15×10^{11} atoms /cm^2 is 61% of the CSI and represents a minimum soil accumulation time of at least 1231 ka.

4.3 Site 3

The site near the hill top has the highest elevation and steepest slope and has the thinnest solum layer (0.9 m). The ^{10}Be concentration reaches a maximum of 10.1×10^8 atoms/g at 57.5 cm, nearly twice the surface concentration of 5.5 $\times 10^8$ atoms/g, and then decreases. The ^{10}Be inventory in the solum is 11% of CSI reflecting the higher soil production rate and represents at least 221 ka of accumulation time

5 Discussion

Soil formation rates calculated using the above ^{10}Be soil inventories and accumulation times and assuming steady state soil thickness (Eq. 2) are shown in Table 4.

Table 4. Soil formation rates (ε) and accumulation times.

Location	^{10}Be* $\times 10^{11}$ (atoms/cm^2)	Soil formation rate (ε) m/Ma	Accumulation time (ka)
Site 1	4.84	1.5 ± 0.6	968
Site 2	6.15	2.6 ± 1.3	1231
Site 3	1.10	5.0 ± 1.2	221

*Cosmogenic steady state ^{10}Be inventory from Eq. 1; 10.0×10^{11} (atoms/cm^2).

At each site the ^{10}Be concentration in the eroded material, η, was taken as the surface 0-25 cm ^{10}Be concentration. The accumulation times range from ~200-1200 ka, and for Sites 1 and 2 are comparable to the 1.39 Ma half-life of ^{10}Be and hence loss of ^{10}Be by decay is significant. Equation 2 corrects for this decay, and hence the most significant source of uncertainty arises from the ^{10}Be fallout rate, which we estimate here to be 20%. The value of η and the soil density have smaller contributions and the net error from the three sources is included in Table 4.

Modern erosion rates (ca. 60 a) calculated using ^{239}Pu [25] at cultivation and grazing sites near our three sites average ~ 750 m/Ma, about 150-500 times higher than the natural soil formation rate. At this rate all the solum will be eroded in 1.2-4.7 ka. The top 0.25 m agriculturally productive layer, however, has a life expectancy of only ~ 340 years. Assuming this erosion rate has been sustained over the last 100 years (European settlement of this catchment commenced in the late 19th century [17]), then soil stripping would have resulted in 3 % (profile 1), 1 % (profile 2) and 6 % (profile 3) reductions in total ^{10}Be inventory, which has a small effect (<3%) on the estimated soil formation rate, and which is within the error of the method.

The observation that ^{10}Be concentrations remain high all the way down to bedrock at sites 2 and 3 in particular might indicate that there has been some loss in solution at the soil-rock boundary. These soils have a pH between 5.5-6.5. Beryllium is present as a hydrolyzed species, (e.g., $BeOH^-$, $Be(OH)_2$) or if humic acid is present as Be humate complexes within this pH range. Both these forms of Be are highly reactive and readily adsorbed onto iron oxy-hydroxides, Aluminium hydroxides and kalonite clay minerals, present in these kandosols [26], and so are likely to be immobile. Acidic soils with pH < 4.1 become under-saturated with respect to $Al(OH)_3$ and release Al^{3+} which competes with other metals, including Beryllium for exchange sites, potentially releasing them into solution [12]. In ultisols, pH < 4, losses of ~50 % meteoric ^{10}Be fallout inventory have been derived from observed ^{9}Be losses in the regolith relative to the primary minerals [27]. This represents an upper limit to the magnitude of meteoric ^{10}Be losses in solution, in the weakly acidic soils encountered in this work.

Mobile colloids can also transport adsorbed metals in aqueous fluids. The presence of natural organic matter (NOM) increases colloid stability and hence decreases the filtering capacity of saprolite to retain metals [28]. After10 cm depth the NOM content of these soils falls below 3%. This would further reduce Be mobility.

A previous study [29] using *in situ* ^{10}Be-^{26}Al, ~270 km northeast of our sites showed a humped soil production function, with optimal soil production under 35-45 cm of soil at sites with similar latitude and climate to ours. Their reported soil production values range from 11.1-23.4 m/Ma for soil mantle thickness of 35-70 cm. The soil production rates of 1.5-5 m/Ma measured here are an order of magnitude below this range, however the soil mantle at 90-354 cm is up to 10 times thicker. This also suggests that soil production slows as the solum layer thickness increases, as a thicker layer would lower the infiltration capacity of groundwater, thus hindering breakdown of the bedrock.

As noted in §2, soil formation rates derived here assume that the only losses of ^{10}Be are due to erosion and decay. If ^{10}Be is also lost by leaving the system in solution in groundwater then the soil formation rates above would be upper limits.

6 Conclusion

The average soil production rate in the Daly Basin, as determined from the natural long term erosion rate, is in the range of 1.5 -5.0 m/Ma. Under cultivation and grazing the erosion rate is 150-500 times higher. The modern soil erosion rates are much higher than the soil formation

rates and hence the present land use practices are unsustainable in the long term. It is therefore prudent that erosion mitigation strategies are prioritized and implemented in the near future.

7 References

1. N. McKenzie, D. Jacquieu, R. Isbell, K. Brown, Australian Soils and Landscapes, An Illustrated Compendium. CSIRO, Canberra, (2004)
2. B. Pillans, Geoderma **80**, 117 (1997)
3. A.M. Heimsath, J.M.A. Chappell, W.E. Dietrich, K. Nishiizumi, R.C. Finkel, Geology **28**, 787 (2000)
4. A.M. Heimsath, J.M.A. Chappell, N.A. Spooner, D.G. Questiaux, Geology **30**, 111 (2002)
5. L.K. Fifield, R.J. Wasson, B. Pillans, J.O.H. Stone, Catena **81,** 32 (2010)
6. D. Lal, B. Peters, In: Site, K. (Ed.), *Handbuch der Physik*. New York, Springer-Verlag, pp. 551–612, (1967)
7. L. Brown, Ann. Rev. Earth and Planetary. Sc. **12,** 39 (1984)
8. J. Chmeleff, F. von Blanckenburg, , K. Kossert, D. Jacob, Nucl. Instrum. Meth. Phys. Res. B **263,** v.2**,** 192 (2010)
9. G. Korschinek, A. Bergmaier, T. Faestermann, U.C. Gerstmann, K. Knie, G. Rugel, A. Wallner, I. Dillmann, G. Dollinger, C.L.von Gostomski,K. Kossert, M. Poutivtsev, A., Remmert, Nucl. Instrum. Meth. Phys. Res. B **268,** 187 (2010)
10. M.J. Pavich, L. Brown, J.W. Harden, J. Klein, R. Middleton, Geochim. Cosmochim. Acta **50,** 1727 (1986)
11. J.A. Graly, L.J. Reusser, P.R. Bierman, Earth and Planetary Science Letters **302,** 329 (2011)
12. J.K. Willenbring, F. von Blanckenburg, Earth Sci. Rev. **98,** 105 (2010)
13. M. Dilshad, Northern Territory Department of Natural Resources, Conservation and the Arts (NRETA).Tech. Report No.18/2008D, Palmerston Australia, ISBN 9781921519048, (2007)
14. D. Wilson, P. Cook, L. Hutley, S Tickell, P. Jolly, Northern Territory Department of Natural Resources the Environment and the Arts, Technical Report No. 17/2006D, Darwin, (2006)
15. Bureau of Meteorology. Climate statistics for Australian locations, Douglas River. http://www.bom.gov.au/jsp/ncc/cdio/cvg/av
16. M. Dilshad, J.A. Motha, L.J. Peel, Aus. J. Exper. Agric. **36,** 1003 (1996)
17. S.J. Lucas, Conservation Commission of Northern Territory, Technical Memorandum No. 10, Darwin, (1984)
18. P.D. Kruse, B.R.Whitehead, C.A. Mulder, Tipperary, Northern Territory. 1:100 000 Geological Series Explanatory Notes, 5170. Northern Territory Geological Survey, Darwin, (1990)
19. B.F. Edmeades. NRETAS, Palmerston, Northern Territory. Technical Report 32/2011D, (2011)
20. J. Stone, Geochim. Cosmochim. Acta **62,** 555 (1998)
21. L.K. Fifield, Rep. Prog. Phys. **62,** 1223 (1999)
22. L.K. Fifield, S.G. Tims, T. Fujioka, W.T. Hoo, S.E. Everett, Nucl. Instrum. Meth. Phys. Res. B **268** 858 (2010)
23. M.C. Monaghan, J. McKean, W. Dietrich, J. Klein, Earth Planet. Sci. Lett. **111**, 483 (1992)
24. E.T. Brown, J.M. Edmond, G.M. Raisbeck, D. Bourlès, F. Yiou, C. Measures, Geochim. Cosmochim. Acta **56,** 1607 (1992)
25. R. Lal, S. Tims, L.K. Fifield, R. Wasson, D. Howe, Nucl. Instrum. Meth. Phys. Res. B, (in press)
26. Y. Takahashi, Y. Minai, S. Ambe, Y. Makide, F. Ambe. Geochim. Cosmochim. Acta **63, v.**6, 815 (1999)
27. A.R. Bacon, D. deB Richter, P.R. Bierman, D.H. Rood, Geology, doi:10.1130/G33449.1 (2012)
28. R. Kretzschmar, W.P. Robarge, A. Amoozegar, Water Resour. Res. **31,** 435 (1995)
29. A.M. Heimsath, D. Fink, G. R. Hancock, Earth Surf. Process. Landforms **34,** 1674 (2009)